The effects of Ni and Au/Ni platings on laser welding of thin sheets

E. Biro, Y. Zhou, and D. C. Weckman[a)]
Department of Mechanical Engineering, University of Waterloo, Waterloo, Ontario N2L 3G1, Canada

K. J. Ely
Edison Welding Institute, 1250 Arthur East Adams Drive, Columbus, Ohio 43210

(Received 14 August 2000; accepted for publication 8 January 2001)

The effects of Ni and Au/Ni plating on laser seam welding of 200 μm thick aluminum, nickel, Kovar, and cold-rolled steel sheet in the lap-joint configuration has been studied. Seam welds were made using a pulsed Nd:YAG laser and a range of weld process conditions. The strength of the welds was characterized using tensile shear tests and all welds were examined metallographically. All material combinations were found to be weldable. The platings were not found to affect the range of process conditions that produced acceptable welds in the nickel, Kovar, and steel specimens. However, the Ni and Au/Ni platings reduced the power density required to form a joint in the aluminum specimens due to the higher absorptivity of Ni. In all cases, the power density which resulted in blowthrough was unaffected by the platings. The strength of the majority of the joints was equivalent to that of the annealed base material. The aluminum weld metal hardness was increased fourfold by alloying from the Ni plating and Au/Ni plating, but this did not affect the tensile shear strength of the joint because failure of the Ni and Au/Ni-plated Al specimens always occurred in the unalloyed softer heat affected zone. Not all of the higher melting point Ni and Au/Ni plating was melted during welding of the Al specimens and significant gas porosity was observed at the interface between the Al weld pool and the unmelted Ni and Au/Ni plating layers. However, this did not affect the tensile shear strengths of the Al welds. A Au/Ni braze joint was observed at the sheet interface adjacent to the fusion boundary of the Au/Ni-plated Ni, Kovar, and cold-rolled steel specimens. This did not affect the strength of the Kovar and cold-rolled steel specimens; however, the Au/Ni braze increased the strength of the Au/Ni-plated Ni specimens to that of the base material.

Key words: Nd:YAG laser welding, electronics, Ni plating, Au plating, nickel, Kovar aluminum

I. INTRODUCTION

In electronic products and devices, base metals such as aluminum, brass, steels, Cu, Kovar, and Ni are often used to make hermetically sealed electronic packaging, interconnections, and assemblies in electronic and optoelectronic devices. While many different joining techniques have been used in electronic packaging, pulsed Nd:YAG laser welding has become the process of choice for most critical devices.[1–5] This is because of the precision and controllability of the process, the ability to weld close to glassed-in metal pins without cracking or remelting of the glass due to the low average heat input rate,[3,5] and the ability to weld a wide range of alloys including aluminum and titanium alloys. It is also possible to laser weld enclosures in an inert gas glovebox environment, thereby eliminating the need and expense of backfilling welded enclosures as a separate operation.[4]

The base materials of hermetic enclosures and other microelectronic components are frequently plated with materials such as Au and Ni. For example, Ni plating is used to improve corrosion, wear, and oxidation resistance of the parts. It is also used as a diffusion barrier between the plated substrate and other precious metal deposits such as Au. Similarly, Au plating is used to reduce contact resistance, to improve oxidation and corrosion resistance, and to improve solderability of the products.[1,6–15] These plating materials can dramatically influence any joining processes which might be used by altering the surface wettability, heat transfer, and optical properties of the materials. They can also significantly affect joint quality. For example, Stockham and Dawes[1] observed significant solidification cracking when CO_2 laser welding electroless or electrolytic Ni-plated Kovar, while Coyle *et al.*,[8] Mizak,[9] and Norrman and Torstensson[10] have found that Au plating above an application specific thickness on Kovar substrates caused solidification cracking in pulsed Nd:YAG laser welds. This has been attributed to the low solubility of Au in Kovar and segregation of the Au along the grain boundaries. In related work with optoelectronic assemblies, Wang *et al.*[11] and Cheng *et al.*[12] reported decreased weld pool dimensions and weld strength with increased Au plating thickness when laser welding Invar specimens in the lap-joint configuration.

Platings can also be beneficial when laser welding. Sakai *et al.*[14,15] have shown that solidification cracking can be prevented when laser seam welding Ni-plated 5052 Al to 1100 Al in the butt-joint configuration by increasing the Ni plating thickness until the weld metal composition was very close to

a)Electronic mail: dweckman@mecheng1.uwaterloo.ca

TABLE I. Alloys, temper conditions, linear tensile strength, and plating thicknesses of the 200 μm thick sheets used in the study.

		Al	Ni	Kovar	CRS
Alloy		1100-H18	200	17Co–29Ni–Fe	C1010
Temper treatment		cold rolled full hard	annealed	annealed	cold rolled
Linear tensile strength (N/mm)		29.0±1.7	86.3±0.8	114.6±2.3	207.0±2.0
Ni plating thickness (μm)		6.0	2.9	3.0	22.1
Au/Ni plating	Ni thickness (μm)	4.3	1.7	3.8	2.6
Au/Ni plating	Au thickness (μm)	2.7	1.3	0.9	1.2

the Al–Al_3Ni eutectic composition. In this case, solidification cracking was observed in thinly or thickly plated Ni specimens, but no cracks were observed when the plating was between 2 and 8 μm thick.

In the present work, the effects of Ni and Au/Ni plating on laser seam welding of 200 μm thick aluminum, nickel, Kovar, and cold-rolled steel sheet in the lap-joint configuration has been studied. Seam welds were made using a pulsed Nd:YAG laser and a range of weld process conditions. The effects of these platings on characteristics such as the minimum power density required for welding, tensile shear strength, and weld quality were examined.

II. MATERIALS AND METHODOLOGY

The base metals used in this study were 200 μm (0.008 in.) thick sheets of 1100 aluminum, nickel, Kovar, and cold-rolled plain-carbon steel (CRS). The alloy, temper condition, and measured linear tensile strength of the sheets are listed in Table I. Some of these sheets were electrolytic sulfamate Ni plated on both sides and some were plated with Ni and then Au. The measured average plating thickness for each material is also listed in Table I. The Ni plating ranged from 1.7 to 22.1 μm in thickness while the Au plating ranged from 0.9 to 2.7 μm in thickness. Nominal thermophysical material properties and absorptivities of the alloys[16,17] are shown in Table II.

Each sheet was sheared into 40 mm×10 mm specimens. Before welding, the specimens were cleaned with acetone followed by a methanol rinse. After cleaning, they were immediately clamped in a lap-joint configuration on the welding jig as shown in Fig. 1 and then laser seam welded. The samples were clamped so that the laser beam was 15° to the normal of the sample to avoid back reflection into the laser. Argon shielding gas was used on both the top and bottom surfaces of the weld.

TABLE II. Nominal thermophysical material properties of the materials used in this study.[16,17]

Material	Melting temperature (°C)	Density (g/cm^3)	Specific heat (J/kg °C)	Thermal conductivity (W/mK)	Absorptivity of 1.06 μm light at 25 °C
Al	660	2.7	900	235	6%
Ni	1455	8.9	435	88	26%
Kovar	1450	7.9	449	16	36%
CRS	1527	6.9	450	46.7	36%
Au	1064	19.3	130	300	5%

The laser seam welds were made using a Lumonics JK702H pulsed Nd:YAG laser with a 600 μm fiber optic delivery system. The system had a 200 mm focal length collimator lens and a 120 mm final focus lens. Independent calibration of the Lumonics JK702H energy meter was performed using an Ophir 1000 W energy meter. Thus, the energy/pulse and peak power actually delivered to the surface of the material was well characterized. The intensity distribution of the laser beam at the focal point was characterized using a rotating-wire-type laser beam analyzer[18] and a LeCroy 9410 digital oscilloscope. As shown in Fig. 2, the beam profile is well approximated by a Gaussian distribution with a $1/e^2$ beam diameter or "spot size", $w_0=413$ μm. For the purpose of this study, the nominal power density was calculated using the relation

$$\mathrm{PD}=\frac{P_p}{(\pi w_0^2/4)}\times 1000, \tag{1}$$

where PD is power density (GW/m^2) and P_p is peak power (W) of each pulse. Most welding laser controls report the laser pulse energy to the operator rather than the nominal power density. The data in this study can be converted from nominal power density (GW/m^2) to pulse energy (J/pulse) by multiplying the reported values by 1.339.

Throughout the experiments, the laser was focused on the top surface of the material and the pulse time, pulse rate, shielding gas flow rate, and welding speed where held at constant preset values (see Table III). A pulse width of 10 ms was chosen based on a study by Weckman and co-workers,[19,20] in which it was found that weld dimensions in 1100 aluminum increased rapidly for the first 2 ms of the pulse and changed little thereafter. This initial transient took place within the first 4 ms when welds were made in less conductive 409 stainless steel. The combination of weld speed and pulse frequency resulted in >50% overlap of in-

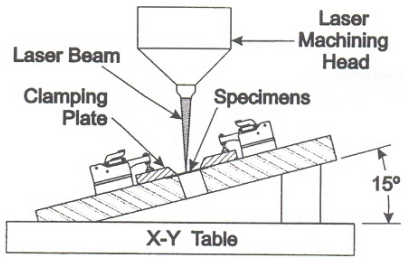

FIG. 1. Schematic of the welding jig used in the experiments.

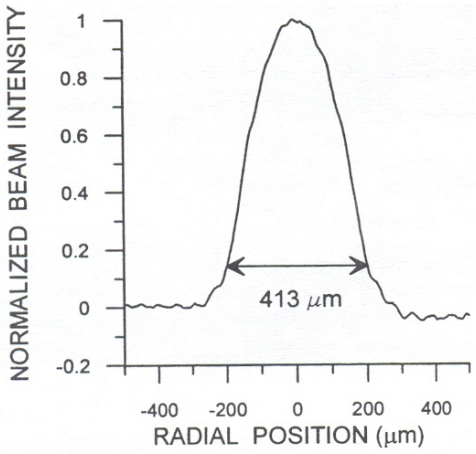

FIG. 2. Measured laser beam intensity profile at the focal point.

dividual spot welds in the seam welds. A 50% spot overlap has been recommended to ensure maximum weld strength in pulsed laser seam welds.[21]

A normal Nd:YAG laser pulse has a high energy spike at the beginning of each pulse[22] which may influence the welding process. To eliminate this spike, temporal pulse shaping was used, that is, each pulse was divided into two sectors, a 0.5 ms leading sector followed by a 9.5 ms main welding sector. Setting the leading sector to 56% of the peak power of the main sector eliminated the initial power spike.

Laser seam welds were produced on the different specimens using a range of peak powers or power densities. The range of power density that produced seam welds is referred to as the process window. The process window extends from the joining threshold, i.e., the minimum power density necessary to form a weld pool large enough to penetrate through the top sheet, across the interface and into the bottom sheet to the power density above which excessive cutting or blowthrough occurs.

Tensile-shear tests were performed on the welded specimens using an Instron 4465 tensile tester with a 5 kN load cell. The geometry of the tensile test samples is shown in Fig. 3. The cross-head speed was 10 mm/min. The tensile-shear test results are presented in units of ultimate strength divided by the width of the weld or linear tensile strength (N/mm). To compare the strength of the joints with that of the base materials, a joint efficiency is calculated by dividing the strength of the joint by the measured strength of the base material. The strength of the base material was measured on the same apparatus and using the same specimen geometry as the tensile-shear specimens.

Transverse sections of all welds were polished, etched, and examined using an optical metallographic microscope.

TABLE III. Preset laser welding parameters used in this study.

Pulse time	10 ms
Pulse rate	5 Hz
Welding speed	1.25 mm/s
% overlap	>50%
Total Ar flow rate	0.47 l/s

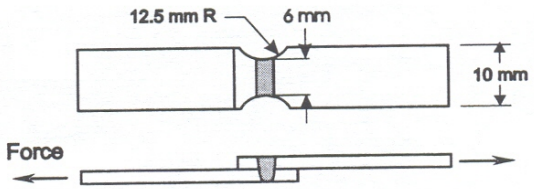

FIG. 3. Schematic of the tensile-shear test specimens.

The aluminum specimens were etched using a solution consisting of 6 ml HBF_4, 1.5 ml HF, and 93 ml H_2O followed by a rinse with 100% HNO_3. The Ni specimens were etched using 80 ml HNO_3, 3 ml HF, and 83 ml H_2O. Finally, the Kovar and CRS specimens were etched using a 2% Nital solution. These etches were found to provide the best microstructural etch for the base metal without excessive etching of the plating materials.

III. RESULTS AND DISCUSSION

A. Aluminum

Figure 4 is a plot of the measured tensile-shear strength of the aluminum specimens versus power density. As may be seen, the Ni or Au/Ni plating significantly affected the joining threshold of the aluminum specimens. The joining threshold of the unplated Al was about 12 GW/m^2. This is in good agreement with the power density for similar welds in 1100 Al reported by Weckman *et al.*[20] Ni-plated Al had a lower joining threshold of about 8.5 GW/m^2 and the Au/Ni-plated Al had an intermediate joining threshold of about 10 GW/m^2. In all three cases of the present study, once the threshold power density was reached, there was a rapid increase in tensile-shear strength to a constant value of about 17 N/mm. The strength remained constant at about 17 N/mm until blowthrough occurred at power densities above about 17 GW/m^2. As indicated in Fig. 4, the maximum strength of all weld specimens was similar to the tabulated strength of annealed 1100 aluminum (1100 O).[16]

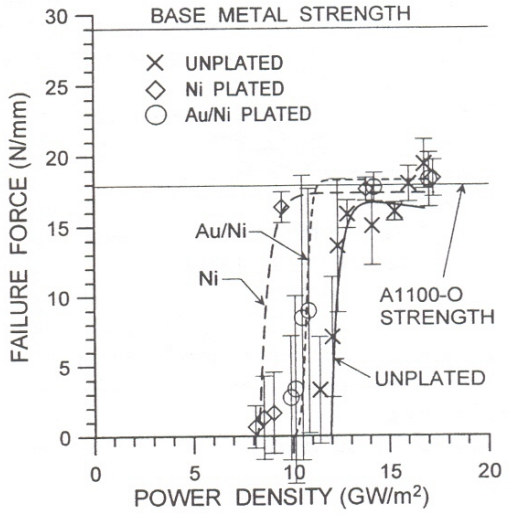

FIG. 4. Measured tensile-shear strengths of the unplated, Ni-plated, and Au/Ni-plated aluminum specimens.

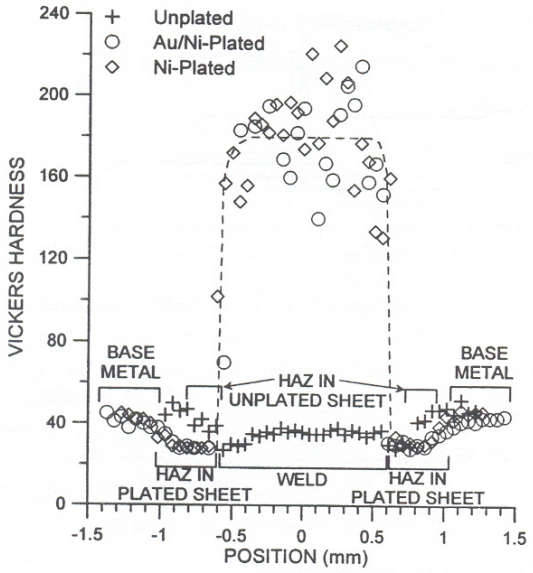

FIG. 5. Microhardness vs position relative to the center of the unplated and plated aluminum weld specimens.

The differences in the threshold power density of the unplated and plated specimens can be related to the characteristics of the aluminum oxide layer on the surface of the uncoated specimens and the Ni and Au/Ni plating layers. Aluminum oxide has a melting point of 2045 °C; approximately 1385 °C above that of Al (660 °C). Thus, a relatively large amount of energy would be required to break through the layers of Al oxide on the incident surface of the top sheet and at the sheet interface before fusion between the top and bottom sheets will be realized. The low absorptivity of the underlying Al (see Table II) means also that higher power densities are required to melt the Al. On the other hand, Ni has a higher absorptivity than Al and a higher melting temperature (1455 °C). Thus, the solid Ni plating will absorb laser energy as the underlying Al melts. This will effectively improve the coupling efficiency between the laser beam during the initial milliseconds of the laser pulse, thus lowering the threshold power density of the Ni-plated Al specimens. Sakai *et al.*[14,15] have also noted improved absorptivity and weld penetration when laser welding Ni-plated versus unplated 5052 and 1100 Al parts in the butt-joint configuration. The presence of the low absorptivity high thermal conductivity Au plating layer on the Au/Ni plated specimens interferes with the improved coupling of the Ni layer. Thus, the threshold power density of the Au/Ni plated specimens falls between the unplated and Ni-plated specimens.

Figure 5 shows Vickers microhardness profiles from unplated and plated aluminum weld specimens. The initial base metal hardness was about 40 Vickers hardness number (VHN). In the unplated specimen, the hardness decreased to about 25 VHN in the heat-affected zone (HAZ) due to annealing of the cold worked sheet. The weld metal hardness is about 30 VHN. The Ni and Au/Ni-plated specimens show a similar drop in hardness in the HAZ due to annealing. However, there is a fourfold increase in hardness in the weld metal due to the solid solution strengthening of the Ni and the dispersion strengthening from the binary Al–Al_3Ni or ternary Al–Al_2Au–Al_3Ni eutectic. A similar increase in weld metal hardness with Ni from Ni plating on 5052 and 1100 Al specimens has also been observed by Sakai *et al.*[14,15]

Energy dispersive x-ray analysis of the Ni-plated Al weld metal indicated a weld metal composition of Al-12.2 wt % Ni. This is very close to the Al–Al_3Ni eutectic composition of Al-11.5 wt % Ni[23] and is likely the reason solidification cracking was not observed in the Ni-plated Al specimens.[14,15] Similarly, the composition of the Au/Ni plated Al specimen weld metal was Al-11.5 wt % Ni-9.4 wt % Au. This is the same composition of the binary Al–Al_3Ni eutectic and just above the binary Al–Al_2Au eutectic composition of Al-7.5 wt % Al_2Au.[23] The overall composition may be very close to the ternary eutectic composition. Again, this is the most likely reason why solidification cracking was not observed in the Au/Ni-plated Al specimens.[14,15]

There were two failure modes observed in the Al tensile shear strength specimens. During the initial transient where the strength was increasing rapidly, the joints failed by shear of the weld throat. During the initial transient, because the weld pool had only just begun to penetrate into the second sheet, the overlap of individual spot welds was small; therefore, the effective weld throat area available to carry the load was small. Once the steady-state strength was reached at higher power densities, however, the effective weld throat was large enough that failure now occurred in the HAZ adjacent to the fusion boundary. This was because of the lower strength of the annealed, unalloyed material in the HAZ relative to the weld metal and cold-rolled base metal (see Fig. 5). While the Ni in the Ni and Au/Ni-plated specimens increased the weld metal hardness by a factor of about four, it did not affect the tensile-shear strength of the welds (see Fig. 4), since all Al welds failed in the much softer HAZ.

The steady-state strength for all Al welded joints was about 17 N/mm. Relative to the measured strength of the base material of 29 N/mm (see Table I) this represents a joint efficiency of 59%. The joint efficiency is low because the strength of the annealed HAZ or weld metal is being compared to that of the cold-rolled base metal. However, the maximum joint efficiency achievable should theoretically be only about 55% (the tensile strength of 1100 O divided by the tensile strength of 1100-H18 Al).[16] On this basis, a joint efficiency of 59% is not unreasonable.

Figures 6 and 7 are photomicrographs of transverse sections through unplated, and Ni-plated aluminum weld specimens, respectively. The microstructural features of the Au/Ni-plated Al weld specimens were very similar to the Ni-plated Al specimens shown in Fig. 7. In all cases, the effective weld throat dimension at the interface was significantly smaller than the width of the fusion boundary in the base material. The reduced weld throat dimensions in these welds are due to differences in the melting temperature and thermal conductivity of the Al relative to its oxide and the plating materials. The fusion boundary in the aluminum sheet extends beyond the original oxide or plating layers because Al melts at a lower temperature ($\approx$660 °C) than its

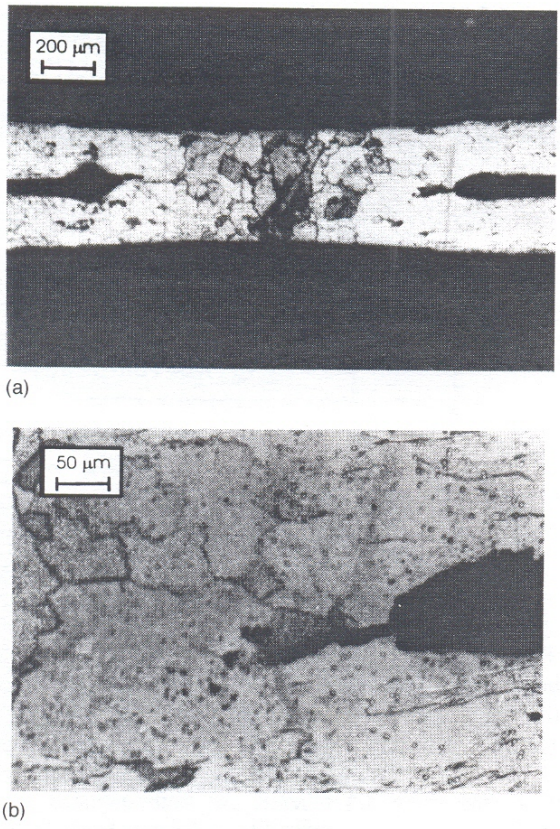

FIG. 6. Transverse sections of a weld in unplated aluminum sheets: (a) the full weld and (b) undisturbed aluminum oxide at the interface near the fusion boundary.

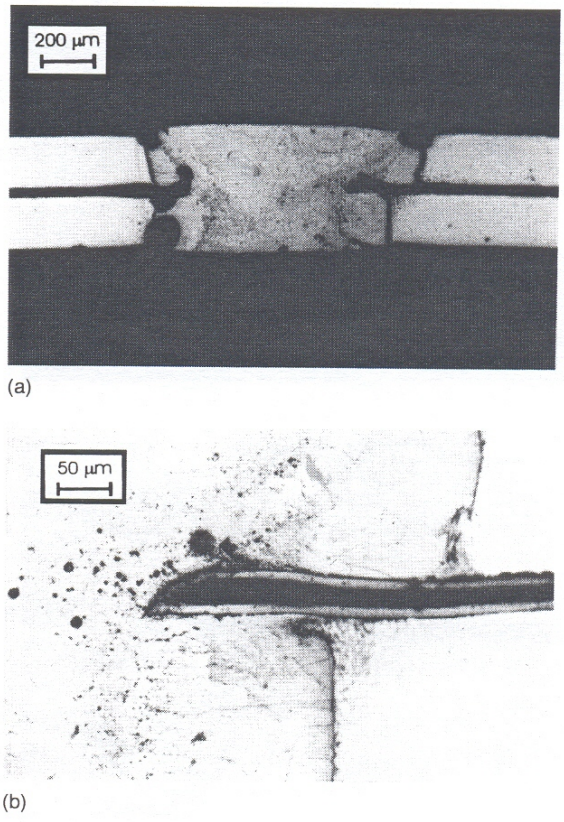

FIG. 7. Transverse section of a weld in Ni-plated aluminum sheets: (a) full weld and (b) unmelted Ni plating at the interface near the fusion boundary.

oxide ($\approx$2045 °C) or either of the plating materials (see Table II). Also, the Al is able to easily conduct any incident heat away from the surface layer into the underlying sheet, thereby limiting the rate of increase of temperature of the surface layer while at the same time melting more of the underlying Al. While this phenomenon reduced the potential width of the weld throat, the actual weld throat was still large enough to resist failure by shear within the weld metal at pull forces that caused the HAZ to fail by shear adjacent to the fusion boundary. Finally, as may be seen in Fig. 7(a), for example, significant gas porosity was observed at the interface between the unmelted Ni and Au/Ni plating layers and the Al weld pool. This porosity did not, however, affect the tensile shear strength of the specimens (see Fig. 4).

B. Nickel

The weldability of the nickel specimens by the pulsed Nd:YAG laser was excellent. As indicated in Fig. 8, the platings did not influence the process window. The joining threshold power density for all specimens was about 6 GW/m^2. This threshold power density was much less than the Al specimens due to the higher absorptivity of Ni relative to Al (see Table II). Above the threshold, the joint strength rose rapidly to full strength and remained at full strength until blowthrough was observed in all specimens above a power density of about 13 GW/m^2.

The Ni welds had good strength compared to the base material. The strengths of the unplated and Ni-plated specimens were the same at about 68 N/mm. Failure of these specimens always occurred by shear in the HAZ adjacent to the fusion boundary. The strength of the base material was about 86 N/mm. This represents a joint efficiency of 79%. The weld strength of the Au/Ni-plated material was 86 N/mm. This represents a joint efficiency of 100%. The rea-

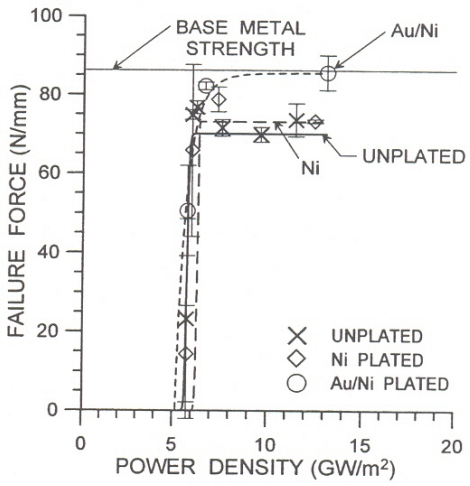

FIG. 8. Measured tensile-shear strengths of the unplated, Ni-plated, and Au/Ni-plated nickel specimens.

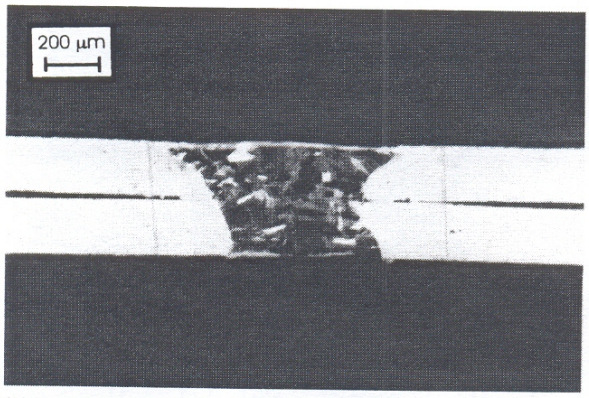

(a)

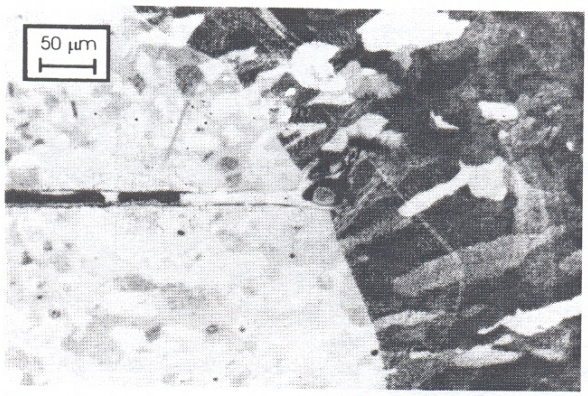

(b)

FIG. 9. Transverse section of a weld in Au/Ni-plated nickel sheets: (a) full weld and (b) brazing at the interface by the plating layers in the HAZ region at the interface.

son for this increase in strength is evident in the photomicrograph of a transverse section of a typical Au/Ni-plated weld specimen shown in Fig. 9. As may be seen, the Au/Ni plating layers at the interface have melted in the HAZ region of the joint due to the lower melting point of the Au/Ni plating relative to the base material (see Table II). Thus, the effective weld throat is increased. All Au/Ni brazed specimens were found to fail by shear in the HAZ or in the stronger base material where the brazing joint first began. In all cases, there was no significant difference in the microhardness of the annealed base metal, the HAZ and the weld metal. The hardness of all specimens was about 150 VHN.

C. Kovar

The weldability of Kovar using the pulsed Nd:YAG laser was excellent. Solidification cracking was not observed in any welds including the Au-plated specimens. This is consistent with the observations of Coyle *et al.*[8] who found that solidification cracking did not occur when the Au plating thickness was less than about 6 μm. Similarly, Norrman and Torstensson[10] did not observe cracking when the Au plating thickness was less than 2.9 μm and Mizik[9] did not observe cracking when the Au plating thickness was less than 1.3 μm. The Au plating thickness on the Au/Ni plated Kovar specimens used in this study was only about 0.9 μm (see

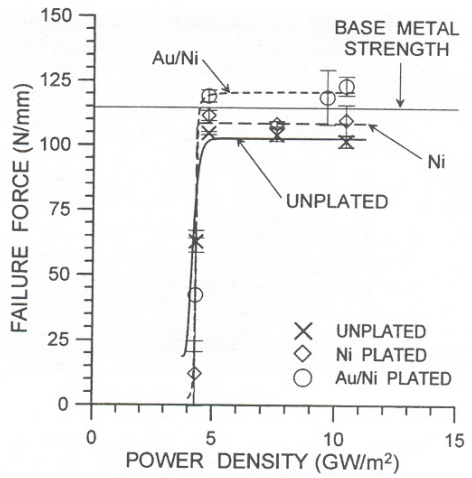

FIG. 10. Measured tensile-shear strengths of the unplated, Ni-plated, and Au/Ni-plated Kovar specimens.

Table I). While there are four Au plating layers in each seam weld in this lap-joint configuration, the total amount of Au was still less than that which would be expected to cause solidification cracking in the Kovar welds.

As shown in Fig. 10, the joining threshold of the Kovar specimens was about 4.3 GW/m^2 for both unplated and plated specimens. This is comparable to the thresholds of the Ni specimens (see Fig. 8). The joint strength of the full penetration welds rose quickly to very high values. Unplated and Ni-plated Kovar had a joint strength of 102 N/mm and all specimens failed by shear in the HAZ adjacent to the fusion boundary. This represents 92% joint efficiency. However, the Au/Ni-plated Kovar was stronger than the other two plated materials having a joint strength of 120 N/mm and a joint efficiency of 100%. This is slightly stronger than the measured strength of the base metal of 114 N/mm. The apparent higher strength is due, however, to experimental scatter of strength data for the base material strength and the weld joint strength. When both data sets are compared, there is a 98% probability that they are the same strength. Blow-through occurred in all specimens at power densities greater than 11 GW/m^2. In all cases, there was no significant difference in the microhardness of the annealed base metal, the HAZ, and the weld metal. The hardness of all specimens was about 160 VHN.

Figure 11 shows a transverse section through a typical Au/Ni-plated Kovar weld specimen. As may be seen in Fig. 11(b), the Au/Ni-plated Kovar welds were as strong as the base material because the plating melted at the interface beyond the fusion boundary, thereby increasing the weld throat. The zone of Au/Ni brazing effectively moves the stress concentration from the HAZ out into the base material. This explains why all of the Au/Ni-plated Kovar specimens failed by shear of the base material where the Au/Ni brazed joint began while the unplated specimens and the Ni-plated specimens failed by shear in the HAZ adjacent to the fusion boundary. Augmentation of joint strength by brazing of the plating at the specimen interface has previously been ob-

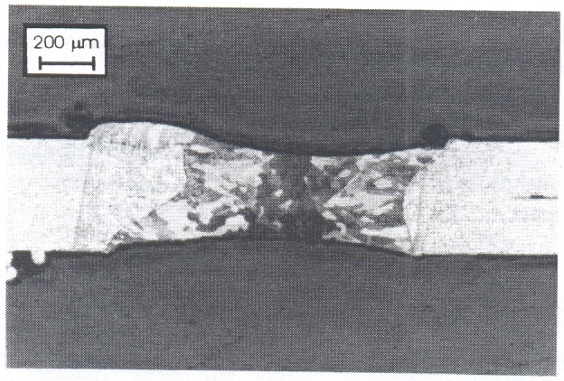

(a)

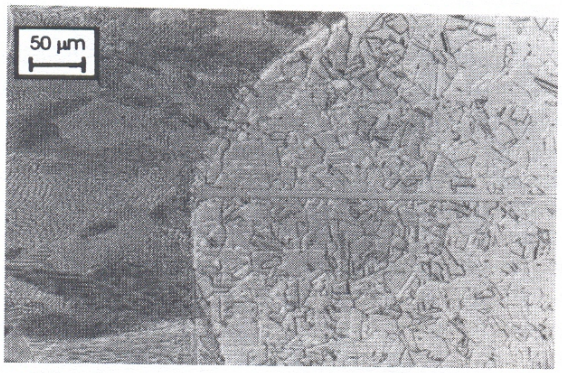

(b)

FIG. 11. Transverse section of a weld in Au/Ni-plated Kovar sheets: (a) full weld and (b) brazing at the interface by the plating layers in the HAZ region at the interface.

served by Stockham and Dawes[1] when laser welding Au or electroless Ni plated Kovar specimens.

D. Cold-rolled steel

The weldability of the CRS samples was excellent. As shown in Fig. 12, the joining threshold of all specimens was the same at about 4 GW/m^2. This was similar to the Ni and

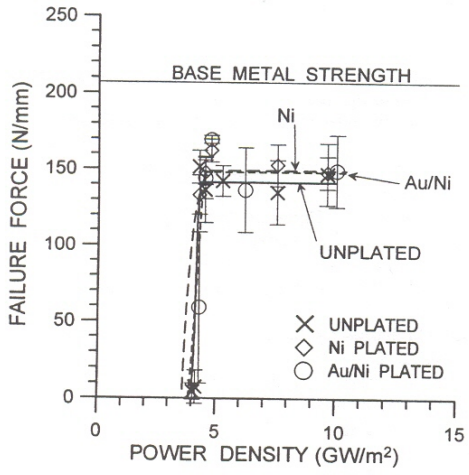

FIG. 12. Measured shear strengths of the unplated, Ni-plated, and Au/Ni-plated cold-rolled steel specimens.

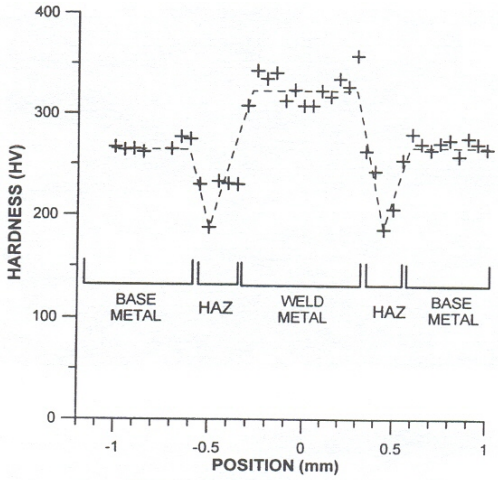

FIG. 13. Microhardness vs position relative to the center of the Au/Ni-plated CRS weld specimen.

Kovar specimens but much lower than the Al specimens due to the significantly higher absorptivity of CRS relative to Al (see Table II). At power densities greater than 4 GW/m^2, the shear strength increased rapidly to values between 130 and 150 N/mm (see Fig. 12). This represents joint efficiencies ranging from 63% for the unplated specimens to 72% for the Ni- and Au/Ni-plated specimens. In all cases, the unplated and Ni-plated specimens failed by shear in the HAZ adjacent to the fusion boundary and the Au/Ni plated specimens failed by shear in the HAZ away from the fusion boundary or in the base metal where the Au/Ni braze first began. Blowthrough occurred in all specimens when the power density exceeded 10 GW/m^2.

Figure 13 shows microhardness values for a Au/Ni-plated CRS steel weld. These values were similar to those of the unplated and the Ni-plated specimens. As seen in Fig. 13, the base metal hardness was about 275 VHN. The hardness decreased in the HAZ to about 200 VHN due to annealing of the cold-worked steel. The weld metal hardness was greatest at about 325 VHN due to transformation hardening of the weld metal.

Figure 14 shows a transverse section of a typical weld in Au/Ni-plated CRS specimen. Similar to the Ni and Kovar specimens, the Au/Ni plating has melted and formed a braze joint at the sheet interface [see Fig. 14(b)]. The braze extended from the fusion boundary into the weld HAZ and is responsible for the observed shift in the failure location from the HAZ adjacent to the fusion boundary to the middle or edge of the HAZ where the braze joint first began.

E. Comparison of the process windows for all materials

The process windows for all of the materials in this study are summarized in Fig. 15. Note that the joining threshold for the Al specimens were significantly higher than all other specimens due to the low absorptivity and high thermal conductivity of Al relative to that of Ni, Kovar, or CRS. Also, as the higher absorptivity Ni plating on the Al base material was able to remain solid for a longer time

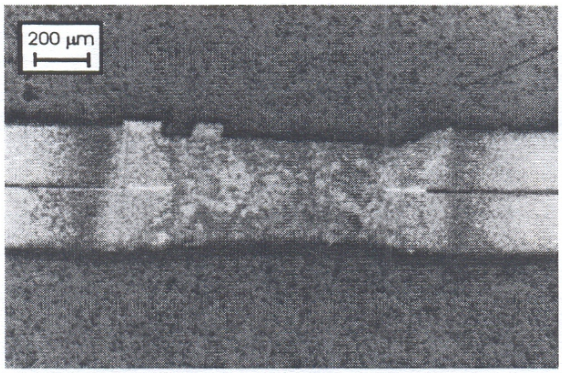

(a)

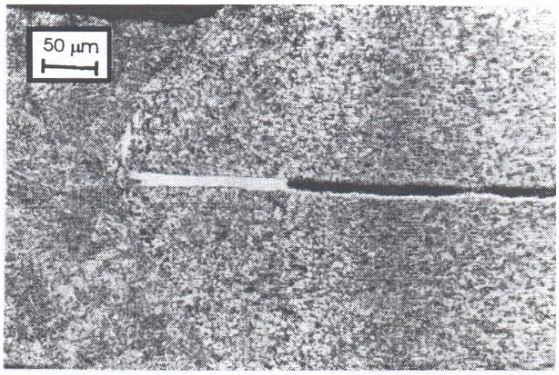

(b)

FIG. 14. Transverse section of a weld in Au/Ni-plated cold-rolled steel: (a) full weld and (b) brazing at the interface by the plating layers in the HAZ region at the interface.

during each laser pulse while the underlying base material was melting, the Ni-plated Al had a significantly lower joining threshold than the unplated Al. Alternatively, the joining threshold of the Ni, Kovar, and CRS specimens were very similar at about 4 GW/m^2 and were not affected by the plating. Finally, the platings had little effect on the power densities above which blowthrough was observed.

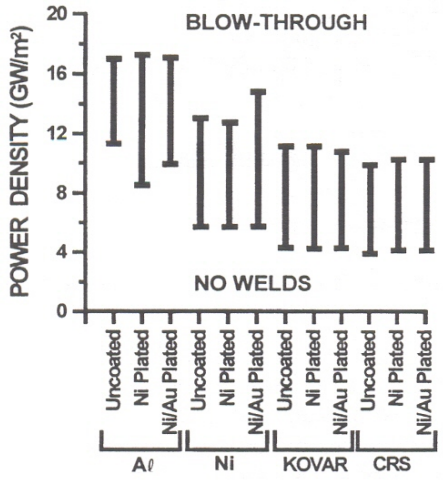

FIG. 15. Ranges of operating power densities that resulted in acceptable welds for all materials studied.

IV. SUMMARY

The effects of Ni-plating and Au/Ni-plating on laser seam welds produced in 200 μm thick aluminum, nickel, Kovar, and cold-rolled steel sheets in the lap-joint configuration have been examined. Welds were produced using a Lumonics JK702H pulsed laser welder and the effects of laser beam intensity and the presence of Ni or Au/Ni plating on joint strength and weld profile were studied.

For all specimens except Al, Ni, or Ni/Au plating was not found to affect the minimum beam intensity necessary for joining. In all cases, a minimum threshold power density was required to initiate joining at the specimen interface. The threshold power density was different for each alloy. Once the weld pool penetrated across the interface into the second sheet, there was a very rapid increase in joint strength to a maximum strength value that was usually less than the base metal strength. This joint strength remained constant with increasing power density until blowthrough or cutting of the sheets occurred. Except for one case, the maximum tensile-shear strength of the joints was not affected by the presence of plating. All unplated and Ni-plated tensile-shear specimens failed by shear in the HAZ adjacent to the fusion boundary where annealing and grain growth had decreased the hardness and strength of the based metal. Au/Ni-plated Ni, Kovar, and CRS specimens exhibited an Au/Ni braze joint at the specimen interface adjacent to the fusion boundary. This caused a shift of the location of tensile-shear failure away from the fusion boundary and into the HAZ or base metal. While there was measurable increase in tensile-shear strength due to the Au/Ni brazing in the Au/Ni-plated Ni specimens, the strength of the Au/Ni-plated Kovar and CRS specimens was not affected by the Au/Ni braze joint at the interface.

ACKNOWLEDGMENTS

This work was supported by the Edison Welding Institute (EWI) and Materials and Manufacturing Ontario (MMO).

[1] N. R. Stockham and C. J. Dawes, "Resistance Seam and Laser Welding of Large Hybrid Metal Packages," Int. J. Hybrid Microelectron. 509–519 (1983).
[2] P. A. Mendicino, "Low Cost Hermetic Sealing of Microwave Modules," Proceedings of the 1984 International Symposium on Microelectronics, Dallas, TX, Sept. 1984, pp. 213–217.
[3] G. A. Knorovsky, P. W. Fuerschbach, S. E. Gianoulakis, and S. N. Burchett, "A Comparison of LBW and GTAW Processes in Miniature Closure Welds," *Trends in Welding Research* (Amer. Soc. for Materials, Metals Park, OH, 1996), pp. 479–485.
[4] R. E. Dickson, "Options in High-Reliability Laser Hermetic Sealing," *Industrial Laser Rev.* **6**(2), 5,6,8 (1991).
[5] P. W. Fuerschbach and D. A. Hinkley, "Pulsed Nd:YAG Laser Welding of Cardiac Pacemaker Batteries with Reduced Heat Input," *Weld. J.* **76**, 103s–109s (1997).
[6] "Golden Rules: Guidelines for the Use of Gold on Connector Contacts," AMP Inc., Technical Report (1996).
[7] T. Iikawa, T. Sakai, S. Okkamoto, K. Natori, and T. Nagai, "Aluminum Alloy Package for Microwave Amplifier," IEEE Trans. Compon., Hybrids, Manuf. Technol. **CHMT-9**, 513–517 (1986).
[8] R. J. Coyle, P. P. Solan, P. J. Sakach, and X-L. Yeh, "Intergranular Embrittlement of Laser Welds by Gold Segregation," *Recent Trends in Welding Science and Technology TWR'89* (ASM Int'l., Materials Park, OH, 1990), pp. 661–665.

[9] P. M. Mizik, "Cracking Investigation of Nd:YAG Laser Welded Gold Plated Glass Sealing Alloys," *Low Thermal Expansion Alloys and Composites* (TMS-AIME, Warrendale, PA, 1992), pp. 139–146.
[10] S. Norrman and P. A. Torstensson, "Sealing of Kovar Hybrid Packages by Laser Welding," *Hybrid Circuits* **8**, 21–23 (1985).
[11] S. C. Wang, C. M. Wang, C. Wang, H. L. Chang, Y. K. Tu, C. J. Hwang, S. Chi, W. H. Wang, Y. D. Yang, and W. H. Cheng, "Effect of Thin Film Coating of Au on Joint Strength in Invar-Invar Packages," J. Electron. Mater. **25**, 1797–1800 (1996).
[12] W-H. Cheng, S-C. Wang, Y-D. Yang, S. Chi, M-T. Sheen, and J-H. Kuang, "Effect of Au Thickness on Laser Beam Penetration in Semiconductor Laser Packages," IEEE Trans. Compon., Packag. Manuf. Technol., Part B **20**, 396–402 (1997).
[13] T. Frech, "Case Study: Welding of Plated Stainless Steel Electronic Packages," Proceedings of the International Conference on Advances in Welding Technology, Joining Applications in Electronics and Medical Devices, Columbus, OH, Sept. 1998, pp. 325–331.
[14] T. Sakai, S. Okamoto and T. Iikawa, "A New Hermetic Sealing Technique of Aluminum Package by Laser," Proceedings of the 36th Electronic Components Conference, Seattle, WA, May 1986, pp. 88–94.
[15] T. Sakai, S. Okamoto, T. Iikawa, T. Sato, and Z. Henmi, "A New Hermetic Sealing Technique for Aluminum Package," IEEE Trans. Compon., Hybrids, Manuf. Technol. **CHMT-10**, 433–436 (1987).
[16] *Metals Handbook* 10th Ed., Vol. 2, "Properties and Selection: Nonferrous Alloys and Special-Purpose Materials" (ASM Int'l, Materials Park, OH, 1990).
[17] W. W. Duley, *Laser Welding* (Wiley, Toronto, ON, 1999).
[18] D. M. Hirak, D. C. Weckman, and H. W. Kerr, "Measuring the Spacial Intensity Distribution of High Power Focused Laser Beams Using a Rotating-Wire Type Laser Beam Analyzer," Meas. Sci. Technol. **5**, 1513–1532 (1994).
[19] J. T. Liu, D. C. Weckman, and H. W. Kerr, "The Effects of Process Variables on Pulsed Nd:YAG Laser Spot Welds: Part I. AISI 409 Stainless Steel," Metall. Trans. B **24B**, 1065–76 (1993).
[20] D. C. Weckman, H. W. Kerr, and J. T. Liu, "The Effects of Process Variables on Pulsed Nd:YAG Laser Spot Welds: Part II. AA 1100 Aluminum and Comparison to AISI 409 Stainless Steel," Metall. Mater. Trans. B **28B**, 687–700 (1997).
[21] C. Marley, "A Guide to Welding with Low-Power YAG Lasers," Weld. J. **75**, 47–50 (1996).
[22] "JK701 and JK702 Nd-YAG Lasers Operation and Maintenance Manual," Lumonics Ltd., England (1992).
[23] *Metals Handbook*, 10th Ed., Vol. 3, "Alloy Phase Diagrams" (ASM Int'l, Materials Park, OH, 1992).